Published in final edited form as:
Wiley Interdiscip Rev Nanomed Nanobiotechnol. 2011 March ; 3(2): 162–173. doi:10.1002/wnan.116.

Revisiting an old friend: manganese-based MRI contrast agents

Dipanjan Pan[*], **Shelton D. Caruthers**, **Angana Senpan**, **Ann H. Schmieder**, **Samuel A. Wickline**, and **Gregory M. Lanza**
Division of Cardiology and C-TRAIN, Washington University School of Medicine, St. Louis, MO 63108, USA

Abstract

Non-invasive cellular and molecular imaging techniques are emerging as a multidisciplinary field that offers promise in understanding the components, processes, dynamics and therapies of disease at a molecular level. Magnetic resonance imaging (MRI) is an attractive technique due to the absence of radiation and high spatial resolution which makes it advantageous over techniques involving radioisotopes. Typically paramagnetic and superparamagnetic metals are used as contrast materials for MR based techniques. Gadolinium has been the predominant paramagnetic contrast metal until the discovery and association of the metal with nephrogenic systemic fibrosis (NSF) in some patients with severe renal or kidney disease. Manganese was one of the earliest reported examples of paramagnetic contrast material for MRI because of its efficient positive contrast enhancement. In this review manganese based contrast agent approaches will be presented with a particular emphasis on nanoparticulate agents. We have discussed both classically used small molecule based blood pool contrast agents and recently developed innovative nanoparticle-based strategies highlighting a number of successful molecular imaging examples.

INTRODUCTION

Molecular imaging has emerged as an interdisciplinary area, which promises to understand the components, processes, dynamics, and therapies of a disease at a biochemical level.[1,2] In general, novel metal-based agents offer unique early detection, diagnosis, and personalized treatment opportunities for a broad range of biomedical imaging modalities. Magnetic resonance imaging (MRI) uses paramagnetic and superparamagnetic metal probes to produce high-resolution noninvasive images that delineate the spatial and temporal nature of abnormal cellular processes in animal models and humans.[2,3] To date, gadolinium (Gd), having a Curie temperature of 17°C and seven unpaired electrons, has been the predominant paramagnetic metal used for MR paramagnetic contrast,[4] but the recent discovery and association with nephrogenic systemic fibrosis (NSF) in some patients with severe renal disease or following liver transplant has fostered concern and Food and Drug Administration (FDA) restrictions on their clinical use.[5–7]

[*]Correspondence to: dpan@cmrl.wustl.edu.

NSF is a rare but potentially harmful side effect which has been creating much controversy in the clinical science of late.[8] Although the first patient diagnosis was made in 1997, the gadolinium-based etiology of the disease was not recognized until 2006. Since then the matter has drawn greater attention from the bench to the clinic, which is reflected in a surge of relevant publications (Figure 1). NSF can be seriously debilitating, leading to fibrotic skin contractures and in extreme cases (5%) result in fractured bones or death. The incurable and nonmitigatable nature of the NSF disease progression has strongly impacted the use of contrast-enhanced MRI guidelines. In some countries in Europe, e.g., Denmark, the issue has such high socioeconomic consequence to the national-run healthcare and welfare systems, the use of such agents is under question and manufactures are being sued to recover economic damages to the state.

The pursuit of alternative, effective ways to achieve personalized molecular imaging has renewed attention given to manganese. Manganese was one of the earliest reported examples of paramagnetic contrast material for MRI because of its efficient positive contrast enhancement.[9–11] Unlike the lanthanides, it is a natural cellular constituent resembling Ca^{2+} that often acts as a regulatory cofactor for enzymes and receptors. However, manganese itself is not out of toxicity issues.[12–15] Through inhalation of manganese-containing dust, toxicity is known to happen in certain occupational settings. The brain is particularly vulnerable to high concentration of manganese exposure. This can cause a neurodegenerative disorder known as ‘manganism’ with characteristics Parkinson-like symptoms. Although not entirely without issues, manganese can be used as an alternative MR contrast agents. Recent study in rats indicated that the optimal dose for MEMRI of the rat visual pathway would be 150–300 nmol *ivit* $MnCl_2$. Higher doses cause toxic reaction, causing retinal ganglion cell (RGC) death, impair active clearance from the vitreous, and loss of Mn^{2+} enhancement throughout the visual pathway.[12] A preclinical toxicological evaluation of 0.5 M solution of Mangascan ethylenediaminetetraacetic acid (Mn-EDTA) and Pentamang diethylene triamine pentaacetic acid (Mn-DTPA) was conducted recently.[13] Rats were given Mangascan (10 ml/kg) or Pentamang (5 mL/kg) i.v. with no toxic influence detected within 2 weeks in the general condition, bone marrow, cardiovascular and central nervous systems, and liver and kidney functions. A very recent report examined the influence of the molecular architecture (linear vs dendritic) and chelator structure on the *in vitro* neurotoxicity in cultured rat primary neurons.[15] A novel hydrosoluble dendritic manganese (II) has been compared with Mn-Linear-DTPA and Mn-DPDP [manganese (II)-dipyridoxaldiphosphate; Teslascan] within a concentration range of 0.1–10 mM. Interpretations suggest that linear-DTPA (diethylene-triaminepentaacetic acid) and dendri-DTPA are relatively well tolerated and it can be concluded that the dendritic architecture is not much more toxic than a linear architecture of the same molecular weight.

This report reviews the growing interest and progress achieved in the field of manganese-based contrast agents for MRI, with a specific focus on the different manganese contrast agent families, their synthetic strategies and properties.

MANGANESE AND MRI PROPERTIES

Typically paramagnetic metals and their compounds having one of more unpaired electrons can be used as MR contrast agents. Paramagnetic metals function by shortening the proton longitudinal relaxation rate ($R1$), which is equal to the relaxation time ($1/T1$). Relaxivity ($r1$) refers to the agent's ability to increase the relaxation rate expressed as (mmol s^{-1}). Essentially a contrast agent with high relaxivity can be detected at lower concentrations, which in turn allows biochemical markers expressed in tissue at μM or nM concentrations to be detected.[1,2] Relaxivity is dependent on a dipolar mechanism of the ion-nuclear distance to the inverse 6th power. As such, metal ions with a large spin number, S, are highly desired for MR contrast agent. Manganese offers a high spin number, long electronic relaxation time and labile water exchange. With five unpaired electrons, manganese is among the best paramagnetic metal for MRI with two manganese (II)-based agents, previously approved for clinical use: the liver-specific Mn-DPDP (Teslascan) and an oral contrast containing manganese (II) chloride (LumenHance). However, these agents have been discontinued since then.

Typically, manganese-based contrast agents can be classified into two broad categories, i.e., small molecule agents (Table 1) and nanoparticulate or macromolecular agents (Table 2) (Figure 2). Manganese mainly in chelated forms has been used as blood pool contrast. In their ionic form (Mn^{2+}) has a very short plasma half-life and not considered as an effective blood pool agent. Small molecule agents were classically entrapped into liposomal formulation, while nanoparticulate agents were purely inorganic or included organic (and/or polymeric) components.

SMALL MOLECULE AGENTS AND THEIR LIPOSOMAL FORMULATION

One of the earliest examples of manganese contrast agents was a solution of manganese(II) chloride.[41] The measured $R1$ value is 8.0 ± 0.1 mM^{-1} s^{-1} at 20 MHz and 37°C[42] and 6.0 mM^{-1} s^{-1} at 40 MHz and 40°C.[43] However, it was found that both i.p. and i.v. injected aquo manganese (II) impart neurotoxicity. The LD50 in mice for manganese (II) is 0.3 mmol kg^{-1} injected intravenously and 1.0 mmol kg^{-1} injected intraperitonially. Orally administered $MnCl_2$ toxicity is ameliorated relative to i.v. concentrations due to the slow rates of metal absorption and presystemic elimination.[44–46] Manganese-enhanced MRI (MEMRI) contrast techniques have been developed for assessing tissue viability as well as providing a surrogate marker of cellular calcium influx and a tracer of neuronal connections. Excellent review articles can be found on MEMRI.[47–51]

Mn-DPDP, approved for liver imaging, has a ratio of LD50 to the dose (range of safety factors) as 540 mmol kg^{-1}, which is higher in comparison to gadolinium diethylenetriaminepentaacetic acid (Gd-DTPA) (60–100).[52] Chelation of the free manganese with DPDP lowers the toxicity and provides selective tissue uptake.[53] The MR relaxivity of Mn-DPDP in aqueous solutions was found to be $r1$ = 2.8 mM^{-1} s^{-1}, $r2$ = 3.7 mM^{-1} s^{-1} with the highest values in kidney ($r1$ = 276.6 mM^{-1} s^{-1} and $r2$ = 640 mM^{-1} s^{-1}). Manganese (II) ions have been entrapped in liposomes to decrease the toxicity in mice relative to free Mn(II), which had $R1$ value of 35.34 mM^{-1} s^{-1} at 20 MHz,[16] and chelated to various

polycarboxylic acid ligands (e.g., EDTA,[50] EDTA-DPP,[50] DTPA, DTPA(PAS)$_2$,[19] and TTHA·[20] for incorporation into lipid bilayer (Table 1). BOM (benzyloxy methyl) groups containing chelates have been used to prepare Mn(II) complexes. These are known to promote a noncovalent interaction with human serum albumin (HSA).[17] The exchange rate of these coordinated water one order of magnitude higher comparison to the exchange rates previously reported for Gd(III) complexes with octadentate ligands. Such fast exchange rates of the coordinated water was exploited in the formation of macromolecular adducts with HSA to attain systems producing high relaxivity values so far reported for analogous Gd(III) systems.

Troughton et al.[18] reported an EDTA-based chelate for Mn(II) containing a diphenylcyclohexyl moiety that is present in the gadolinium-based agent MS-325. This moiety is known to bind noncovalently to serum albumin. The concept of Mn-based *in vivo* imaging was tested in a rabbit model of carotid artery injury.

Manganese in bivalent form has been inserted to porphyrins, such as sulfonatoporphyrins, where it undergoes rapid oxidation to Mn(III) (Figure 3).[21] Manganese (III) tetra-(4-sulfonatophenyl) porphyrin (TPPS$_4$) was one of the earliest examples of sulfonatoporphyrins followed by analogs with progressively fewer sulfonate functionalities (TPPS$_3$, TPPS$_2$, Table 1).[22,23] Similar manganese complexes include UROP-1,[24] mesoporphyrin, hematoporphyrin[25,26], and ATN-10.[27] *Recently, the performance of a potentially tumor-seeking MR agent* α-Aqua-13, 17-bis(1-carboxypropionyl)carbamoyl ethyl-3,8-bis(1-phenethyloxyethyl)-β-hydroxy-2,7,12, 18-tetramethyl-porphyrinato manganese (III) (HOP-8P) was evaluated in a tumor-bearing mouse model.[28] Paramagnetic manganese chelated within the porphyrin-ring has been reported to provide sustained tumor enhancement up to at least 24 h following contrast injection in a tumor-bearing (SCC-VII) mice.[54]

Lippard et al. reported an interesting mechanism for ion sensing by MRI.[55] The mechanism shows competitive displacement of paramagnetic ions, which results in alteration of solvent interaction parameters and changes in relaxivity and MRI contrast. As a specific example, they demonstrate a Ca-dependent displacement of manganese(II) ions bound to EGTA [ethylene glycol bis(β-aminoethyl ether)-*N,N,N′,N′*-tetraacetic acid] and BAPTA (1,2-bis(o-aminophenoxy)-ethane-*N,N,N′,N′*-tetraacetic acid) ligands results in a *T*1w MRI signal increase based.

Inorganic Particle Approach

Shapiro and Koretsky have successfully utilized insoluble, inorganic manganese oxide particles (i.e., MnO, MnO_2, and Mn_3O_4) and manganese carbonate ($MnCO_3$) in bulk inorganic powder form, as convertible contrast agents for molecular and cellular MRI agents (Figure 4). These Mn particles are typically water insoluble at neutral pH and are formulated into nano- or microparticles. These manganese oxide particles have high magnetic susceptibilities that produce dark contrast when using *T*2*-weighted[1,2] MRI pulse sequences. However, after cellular internalization and localization within endosomes and/or lysosomes, the particles are degraded by the abundant proteolytic enzymes in the

predominantly acidic environment, releasing Mn^{2+} ions, which are strong $T1$ MRI contrast agents.[29]

NANOPARTICLE AND MACROMOLECULAR AGENTS

Manganese-Doped Iron Oxide Nanoparticles

Leung et al.[30] prepared one-dimensional Mn-Fe oxide composite nanostructures of 400–1000 nm sizes in needle, rod, and wire forms. The nanostructures were synthesized by the treatment of $MnFe_2O_4$ nanoparticles with cystamine resulting in an organization of the manganese-doped iron oxide nanoparticles. *In vitro* studies showed that the nanostructures could be transported into the cells of monocyte/macrophage cell line (RAW264.7) with negligible impact on cell viability at labeling concentration <50 μg/mL. Unfortunately, their MR properties were not promising. The results from 1.5 T MR indicated that the $T2$ relaxivities ($r2$) for nanoneedles, nanorods, and nanowires were 20.81 ± 0.58, 8.10 ± 0.31, and 6.62 ± 0.42 $mM^{-1}s^{-1}$, respectively, which were lower than the corresponding iron oxide nanoparticle derivatives [e.g., VSOP-C184 and SHU-555C (Supravist)]. It is postulated that the formation of the larger nanostructures led to lower MR relaxivities.[30]

Ultrasensitive MRI contrast agents for liver imaging were developed based on manganese-doped superparamagnetic iron oxide (Mn-SPIO) nanoparticles. Hydrophobically modified Mn-SPIO nanoparticles were incorporated within self-assembled block copolymer (mPEG-*b*-PCL) micelles (mean diameter ~80 nm). At room temperature, Mn-SPIO nanoparticles exhibited superparamagnetism. At the 1.5 T, the clustering micelles had a $T2$ relaxivity of 270 (Mn + Fe) mM^{-1} s^{-1}, which was much higher than single Mn-SPIO nanoparticle in a lipid-PEG micelle. This resulted in significant liver contrast with signal intensity decreased of ~80% in 5 min after intravenous administration. The strongly enhanced-MRI negative contrast liver images were highly prolonged and offered sensitive detection of minute liver lesions.[31] Similarly, multifunctional magneto-polymeric nanohybrids (MMPNs) have been synthesized using ultrasensitive $MnFe_2O_4$ nanocrystals, chemotherapeutic agents, and encapsulating amphiphilic block copolymers for targeted MR detection and treatment of breast cancer.[32] However the MRI contrast mechanism for manganese ferrite nanoparticles are quite different than the other agents (i.e., MnO based agents) discussed in this review. They are essentially $T2$ contrast agents for MRI. They provide ferromagnetic properties and shorten the relaxation time of the water protons by providing a localized magnetization when applying the external magnetic field.

Manganese-Based Clusters

Manganese-based oxo clusters [e.g., $Mn_{12}O_{12}(O_2C\ CH_3)_{16}(H_2O)_4$] are another class of important contrast agents of inorganic nature. They are typically considered as prototypical ‘Single Molecule Magnet’ (SMM) because at low temperature the high spin state ($S = 10$) and anisotropy results in favorable magnetic properties.[56–59] Stoll et al. showed that manganese-oxo clusters had promise as an MRI contrast agent. Moreover, their MR and water solubility properties improved when they were incorporated onto the surface of polymer (e.g., polystyrene) beads (Figure 5).[33]

Li et al. reported the synthesis and MR evaluation of two Mn(II)-monosubstituted polyoxometalates (MnPOMs), $MnSiW_{11}$, and MnP_2W_{17}.[34] These agents were evaluated by *in vivo* and *in vitro* experiments as the candidates of tissue-specific MRI contrast agents. The measured relaxivities exhibited improved relaxation ability in comparison with Gd-DTPA. *In vivo* MR imaging in healthy rats demonstrated signal enhancement in liver and kidney, suggesting that with appropriate chemical modification, these two agents could be used as promising liver- and kidney-specific MRI contrast agents.

Manganese-Organic Frame Work

Manganese-based core-shell nanoscale metal-organic frameworks (NMOFs) were synthesized by Wenbin Lin's group.[35] Mn-NMOFs comprised of terephthalic acid (BDC) and trimesic acid (BTC) bridging ligands were synthesized by reverse-phase microemulsions. Nanorods of $Mn(BDC)(H_2O)_2$ were synthesized by stirring a cetyl trimethylammonium bromide (CTAB)/1-hexanol/*n*-heptane/water microemulsion containing an equimolar $MnCl_2$ and $[NMeH_3]_2(BDC)$. Similarly, nanoparticles of $Mn_3(BTC)_2(H_2O)_6$ were prepared in a CTAB/1-hexanol/isooctane/water microemulsion mixture containing a $Na_3(BTC)/MnCl_2$ molar ratio of 2:3. The particle morphology was tested by transmission electron microscopy (TEM) and scanning electron microscopy (SEM) techniques, which revealed that the particles adopt uniform spiral rod morphology with diameter 50–100 nm and lengths 1–2 μm. The stability of the particles was achieved by a silica coating. Polyvinyl pyrrolidone (PVP)-modified particles underwent base-catalyzed condensation of tetraethyl orthosilicate (TEOS) to generate a thin layer of silica shell, which provided a chemical foundation for functionalization with a fluorophore (rhodamine B) and a cell-targeting cyclic peptide (cRGDfk), selectively binds $\alpha_v\beta_3$ integrin for targeting angiogenic cancers cells. Rhodamine B- and c(RGDfK)-coupled particles demonstrated effective target-specific MR imaging to cancer cells *in vitro*, which was corroborated by optical imaging. Although the $r1$ values exhibited by the Mn-NMOFs were unexceptional, their high water solubility delivered large doses of Mn^{2+} ions inside cells. *In vitro* and *in vivo* results both suggested that the silica-coated particles could deliver Mn^{2+} to sites of interest for high $T1$-weighted contrast enhancement.

Manganese Oxide Nanoparticle-Based Approach

Biocompatible MnO nanoparticles were prepared for MR imaging to elicit bright signal enhancement and fine anatomic detail in the $T1$-weighted MR image of a mouse brain. Uniformly sized MnO nanoparticles were dispersed in nonpolar organic solvent by the thermal decomposition of Mn-oleate complex was encapsulated in a polyethyleneglycol (PEG)-phospholipid shell for increased water solubility and improved biocompatible. These particles were shown to target breast cancer cells in a metastatic tumor in brain.[36] In another recent report,[37] the relaxivity of MnO nanoparticles was altered by manipulating the size and curvature of the particles. Manganese oxide nanoparticles (20 nm) stabilized by oleic acid manganese oxide nanoparticles (MONs) as well as water-dispersible manganese oxide nanoparticles (WMONs) were prepared and encapsulated with poly(ethylene glycol) phospholipids. The selective removal of the MnO phase from the WMONs created hollow manganese oxide nanoparticles (HMONs). These HMONs were loaded with therapeutic

agents and retained efficient cellular uptake illustrating the potential of bifunctional theragnostic approach.

Organic or Polymeric Nanoparticle-Based Approach

Manganese (III)-labeled nanobialy, a 'soft-type' toroidal biconcave particle, has potential as targeted MR theranostic agent.[39] Nanobiays are formed through spontaneous self-assembly of amphiphilic hyperbranched polyethylenimine particle size (180–200 nm) with low polydispersity (Figure 6). The 'Bialys' presented Mn(III) in a kinetically stable, manganese protoporphyrin-coupled complex directly exposed to the surrounding water producing ionic $r1$ and $r2$ relaxivities of 3.7 ± 1.1 $mmol^{-1}$ s^{-1} and 5.2 ± 1.1 $mmol^{-1}$ s^{-1} per Mn ion and particulate relaxivities of 612,307 ± 7213 $mmol^{-1}$ s^{-1} and 866,989 ± 10, 704 $mmol^{-1}$ s^{-1} per particle, respectively. The theragnostic potential of nanobialy's was illustrated through targeted Mn MR imaging *in vitro* using antifibrin monoclonal targeting to fibrin-rich clots the efficient (98%) synthetic incorporation and *in vitro* dissolution retention (80%) of chemotherapeutic compounds (doxorubicin and camtothecin).

Alternative 'soft-particle' approaches included manganese oxide and manganese oleate nanocolloids[38] (particle size >120 nm), which were developed by incorporating manganese (II) oxide (10 nm) particles or manganese (II) oleate within a hydrophobic core matrix encapsulated by phospholipids. Specific homing ligands, including antifibrin antibodies and αvβ3 intergrin antagonists,[1,2] were presented on the functionalized surface providing high avidity and sensitivity for molecular imaging with MRI (excellent 'stick and stay' quality).

MR experiments at 3.0 T magnetic field demonstrated high-resolution $T1$w molecular imaging with manganese oxide nanocolloids (ManOC) and manganese oleate nanocolloids (ManOL) in suspension and bound to fibrin. The ionic $r1$ relaxivities of ManOC and ManOL were 4.1 ± 0.9 $mmol^{-1}$ s^{-1} and 20.4 ± 1.1 ($mmol^{-1}$ s^{-1} per Mn, while the particulate relaxivities were 85,099 $mmol^{-1}$ s^{-1} and 631,208 $mmol^{-1}$ s^{-1} per particle, respectively. The ionic $r2$ relaxivities of ManOC and ManOL were 18.9 ± 1.1 $mmol^{-1}$ s^{-1} and 65.6 ± 0.9 $mmol^{-1}$ s^{-1} per Mn, and the $r2$ relaxivities were 395,410 $mmol^{-1}$ s^{-1} and 2,028,925 $mmol^{-1}$ s^{-1} per particle, respectively. The specific relaxivities were found to be markedly and unexpectedly higher for the ManOL as compared to the ManOC. Fibrin-rich clots were targeted in vitro with fibrin-specific monoclonal antibodies revealed increased $T1$w images of the targeted specimens, yielding signal intensities (75 ± 20 a.u. and 95 ± 19 a.u., respectively) versus the control nanocolloids (32 ± 07 a.u.), and background air (7 ± 4 a.u.). These results suggest that ManOL has outstanding potential for imaging intravascular microthrombus associated with rupture atherosclerotic plaque, and may provide adequate contrast to detect the very sparse biosignatures of angiogenesis in cancer and vascular diseases (Figure 7).

Examples of the polymeric and dendritic manganese contrast agents are also known in the literature.[15,40] Steibel et al.[40] reported the development of a dendritic agent based on novel hydrophilic dendritic Mn(II) complex 1 derived from DTPA for MEMRI experiments for brain imaging. These complexes exhibit no *in vitro* neuronal toxicity at concentration ~1 mM. The $T1$ relaxivity of one of the complexes were found to be 4.2 mM^{-1} s^{-1}, which was higher than that of the commercial MRI contrast agents Gd-DTPA.

CONCLUSION

Clearly, manganese-based agents have continued to be developed and new nanotechnologies have great promise for achieving high MR contrast. They have the potential of reducing the risk of toxicity or intolerance due to the release of free metal. Although better patient stratification and gadolinium chelation chemistry may prevent the acute induction of NSF, the potential avoidance of NSF occurring in the future among patients given lanthanides, particularly repeat doses, can be only speculated upon. The need to further lower or eliminate gadolinium exposure must be considered a high priority for the molecular imaging community. Manganese-based technologies offer an alternative pathway that may achieve the success that gadolinium-based agents have heretofore enjoyed.

REFERENCES

1. Pan D, Lanza GM, Wickline SA, Caruthers SD. Nanomedicine: perspective and promises with ligand-directed molecular imaging. Eur J Radiol. 2009; 70:274–285. [PubMed: 19268515]
2. Pan D, Caruthers SD, Chen J, Winter PM, Senpan A, Schmieder AH, Wickline SA, Lanza GM. Nanomedicine strategies for molecular targets with MRI and optical imaging. Future Med Chem. 2010; 2:471–491. [PubMed: 20485473]
3. Massoud TF, Gambhir SS. Molecular imaging in living subjects: seeing fundamental biological processes in a new light. Genes Dev. 2003; 17:545–580. [PubMed: 12629038]
4. Chan KW, Wong W-T. Smallmolecular gadolinium(III) complexes as MRI contrast agents for diagnostic imaging. Coord Chem Rev. 2007; 17:2428–2451.
5. Sieber MA, Steger-Hartmann T, Lengsfeld P, Pietsch H. Gadolinium-based contrast agents and NSF: evidence from animal experience. J Magn Reson Imaging. 2009; 30:1268–1276. [PubMed: 19938039]
6. Prince MR, Zhang HL, Prowda JC, Grossman ME, Silvers DN. Nephrogenic systemic fibrosis and its impact on abdominal imaging. Radiographics. 2009; 29:1565–1574. [PubMed: 19959508]
7. Idée JM, Port M, Dencausse A, Lancelot E, Corot C. Involvement of gadolinium chelates in the mechanism of nephrogenic systemic fibrosis: an update. Radiol Clin North Am. 2009; 47:855–869. [PubMed: 19744600]
8. Thomsen HS. Nephrogenic systemic fibrosis: history and epidemiology. Radiol Clin North Am. 2009; 47:827–831. [PubMed: 19744597]
9. Lauterbur, PC.; Dias, MH.; Rudin, AM. Frontiers of Biological Energetics. Dutton, PL.; Leigh, JS.; Scarpa, A., editors. New York: Academic Press; 1978. p. 752-759.
10. Mendonca-Dias MH, Gaggelli E, Lauterbur PC. Paramagnetic contrast agents in nuclear magnetic resonance medical imaging. Sem Nucl Med. 1983; 13:364–376.
11. Wendland MF. Applications of manganese-enhanced magnetic resonance imaging (MEMRI) to imaging of the heart. NMR Biomed. 2004; 17:581–594. [PubMed: 15761947]
12. Thuen M, Berry M, Pedersen TB, Goa PE, Summerfield M, Haraldseth O, Sandvig A, Brekken C. Manganese-enhanced MRI of the rat visual pathway: acute neural toxicity, contrast enhancement, axon resolution, axonal transport, and clearance of Mn(2+). J Magn Reson Imaging. 2008; 28:855–865. [PubMed: 18821627]
13. Churin AA, Karpova GV, Fomina TI, Vetoshkina TV, Dubskaia TIu, Voronova OL, Filimonov VD, Belianin ML, Usov VIu. Preclinical toxicological evaluation of Pentamang and Mangascan. Eksp Klin Farmakol. 2008; 71:49–52. [PubMed: 18819441]
14. Santamaria AB. Manganese exposure, essentiality & toxicity. Indian J Med Res. 2008; 128:484–500. [PubMed: 19106442]
15. Bertin A, Michou-Gallani A-I, Gallani JL, Felder-Flesch D. *In vitro* neurotoxicity of magnetic resonance imaging (MRI) contrast agents: Influence of the molecular structure and paramagnetic ion. Toxicol in Vitro. 2010; 24:1386–1394. [PubMed: 20460148]

16. Unger E, Fritz T, Shen DK, Wu G. Manganese-based liposomes: comparative approach. Invest Radiol. 1993; 28:933–938. [PubMed: 8262748]
17. Aime S, Anelli PL, BOtta M, Brocchetta M, Canton S, Fedeli F, Gianolio E, Terreno E. Relaxometric evaluation of novel manganese (II) complexes for application as contrast agents in magnetic resonance imaging. J Biol Inorg Chem. 2002; 7:58–67. [PubMed: 11862541]
18. Troughton JS, Greenfield MT, Greenwood JM, Dumas S, Wiethoff AJ, Wang J, Spiller M, McMury TJ, Caravan P. Synthesis and evaluation of a high relaxivity manganese(II)-based mri contrast agent. Inorg Chem. 2004; 43:6313–6323. [PubMed: 15446878]
19. Schwendener RA, Wüthrich R, Duewell S, Wehrli E, von Schulthess GK. A pharmacokinetic and MRI study of unilamellar gadolinium-, manganese-, and iron-DTPA-stearate liposomes as organ-specific contrast agents. Invest Radiol. 1990; 25:922–932. [PubMed: 2394576]
20. Rongved P, Klaveness J. Water-soluble polysaccharides as carriers of paramagnetic contrast agents for magnetic resonance imaging: synthesis and relaxation properties. Carbohydr Res. 1991; 214:315–323. [PubMed: 1769023]
21. Buchler, JW. Synthesis and properties of metalloporphyrins. In: Dolphin, D., editor. The Porphyrins. Vol. I A. New York: Academic Press; 1979. p. 389-483.
22. Place DA, Faustino PJ, Berghmans KK, van Zijl PCM, Chesnick AS, Cohen JS. Magn Reson Imaging. 1992; 10:919–928. [PubMed: 1461089]
23. Fiel RJ, Musser DA, Mark EH, Mazurchuk R, Alletto J. J Magn Reson Imaging. 1990; 8:255–259.
24. Schmiedl UP, Nelson JA, Robinson DH, Michalson A, Starr F, Frenzel T, Ebert W, Schuhmann-Giampieri G. Invest Radiol. 1993; 28:925–932. [PubMed: 8262747]
25. Fawwaz RA, Winchell HS, Frye F, Hemphill W, Lawrence JH. Localization of 58Co and 65Zn-hematoporphyrin complexes in canine lymph nodes. J Nucl Med. 1969; 10:581–585. [PubMed: 5797845]
26. Fawwaz RA, Hemphill W, Winchell HS. Potential use of Pd-porphyrin complexes for selective lymphatic ablation. J Nucl Med. 1971; 12:231–236. [PubMed: 5580839]
27. Fujimori H, Matsumura A, Yamamoto T, Shibata Y, Yoshizawa T, Nakagawa K, Yoshii Y, Nose T, Sakata I, Nakajima S. Tumor specific contrast enhancement study of Mn-metalloporphyrin (ATN-10)—comparison of rat brain tumor model, cytotoxic and vasogenic edema models. Acta Neurochir. 1997; 70:167–169.
28. Takehara Y, Sakahara H, Masunaga H, Isogai S, Kodaira N, Sugiyama M, Takeda H, Saga T, Nakajima S, Sakata I. Assessment of a potential tumor-seeking manganese metalloporphyrin contrast agent in a mouse model. Magn Reson Med. 2002; 47:549–553. [PubMed: 11870842]
29. Shapiro EM, Koretsky AP. Convertible manganese contrast for molecular and cellular MRI. Magn Reson Med. 2008; 60:265–269. [PubMed: 18666118]
30. Leung KC, Wang YX, Wang H, Xuan S, Chak CP, Cheng CH. Biological and magnetic contrast evaluation of shape-selective Mn-Fe nanowires. IEEE Trans Nanobiosci. 2009; 2:192–198.
31. Lu J, Ma S, Sun J, Xia C, Liu C, Wang Z, Zhao X, Gao F, Gong Q, Song B, Shuai X, Ai H, Gu Z. Manganese ferrite nanoparticle micellar nanocomposites as MRI contrast agent for liver imaging. Biomaterials. 2009; 30:2919–2928. [PubMed: 19230966]
32. Yang J, Lee CH, Ko HJ, Suh JS, Yoon HG, Lee K, Huh YM, Haam S. Multifunctional magneto-polymeric nanohybrids for targeted detection and synergistic therapeutic effects on breast cancer. Angew Chem Int Ed Engl. 2007; 46:8836–8839. [PubMed: 17943947]
33. Mertzman JE, Kar S, Lofland S, Fleming T, Keuren EV, Tong YY, Stoll SL. Surface attached manganese–oxo clusters as potential contrast agents. Chem Commun. 2009; 45:788–790.
34. Li Z, Li W, Li X, Pei F, Wang X, Lei H. Mn(II)-monosubstituted polyoxometalates as candidates for contrast agents in magnetic resonance imaging. J Inorg Biochem. 2007; 101:1036–1042. [PubMed: 17524483]
35. Taylor KM, Rieter WJ, Lin W. Manganese-based nanoscale metal-organic frameworks for magnetic resonance imaging. J Am Chem Soc. 2008; 130:14358–14359. [PubMed: 18844356]
36. Na HB, Lee JH, An K, Park YI, Park M, Lee IS, Nam DH, Kim ST, Kim SH, Kim SW, Lim KH, Kim KS, Kim SO, Hyeon T. Development of a T1 contrast agent for magnetic resonance imaging using MnO nanoparticles. Angew Chem Int Ed Engl. 2007; 46:5397–5401. [PubMed: 17357103]

37. Shin J, Anisur RM, Ko MK, Im GH, Lee JH, Lee IS. Hollow manganese oxide nanoparticles as multifunctional agents for magnetic resonance imaging and drug delivery. Angew Chem Int Ed Engl. 2009; 48:321–324. [PubMed: 19040234]
38. Pan D, Senpan A, Caruthers SD, Williams TA, Scott MJ, Gaffney PJ, Wickline SA, Lanza GM. Sensitive and efficient detection of thrombus with fibrin-specific manganese nanocolloids. Chem Commun (Camb). 2009:3234–3236. [PubMed: 19587924]
39. Pan D, Caruthers SD, Hu G, Senpan A, Scott MJ, Gaffney PJ, Wickline SA, Lanza GM. Ligand-directed nanobialys as theranostic agent for drug delivery and manganese-based magnetic resonance imaging of vascular targets. J Am Chem Soc. 2008; 130:9186–9187. [PubMed: 18572935]
40. Steibel BA, Michou-Gallani AI, Gallani JL, Felder-Flesch D. Development of a dendritic manganese-enhanced magnetic resonance imaging (MEMRI) contrast agent: synthesis, toxicity (in vitro) and relaxivity (in vitro, in vivo) studies. Bioconjug Chem. 2009; 20:760–767. [PubMed: 19368343]
41. Lauterbur, PC.; Mendonc¸a-Dias, HM.; Rudin, AM. Augmentation of tissue water proton spin-lattice relaxation by in vivo addition of paramagnetic ions. In: Dutton, PL.; Leigh, JS.; Scarpa, A., editors. Frontiers of Biological Energetics. Vol. 1. New York: Academic Press; 1978. p. 752-759.
42. Chen C-W, Cohen JS, Myers CE, Sohn M. Paramagnetic metalloporphyrins as potential contrast agents in NMR imaging. FEBS Lett. 1984; 168:70–74. [PubMed: 6705923]
43. Kreft BP, Baba Y, Tanimoto A, Finn JP, Stark DD. Orally administered manganese chloride: enhanced detection of hepatic tumors in rats. Radiology. 1993; 186:543–548. [PubMed: 8421762]
44. Greenberg DM, Copp DH, Cuthbertson EM. Studies in mineral metabolism with the aid of artificial radioactive isotopes. VII. The distribution and excretion, particularly by way of the bile, of iron, cobalt, and manganese. J Biol Chem. 1943; 147:749–756.
45. Kojima S, Hirai M, Kiyozumi M, Sasawa Y, Nakagawa M, Shin-o T. Studies on poisonous metals. X. Metabolic fate of manganese after oral administration of excessive manganese chloride in rats. Chem Pharm Bull. 1983; 31:2459–2465. [PubMed: 6640808]
46. Sandström B, Davidsson L, Cederblad Å, Eriksson R, Lönnerdal B. Manganese absorption and metabolism in man. Acta Pharmacol Toxicol. 1986; 59:60–62.
47. Koretsky AP, Silva AC. Manganese-enhanced magnetic resonance imaging (MEMRI). NMR Biomed. 2004; 17:527–531. [PubMed: 15617051]
48. Lee JH, Koretsky AP. Manganese enhanced magnetic resonance imaging. Curr Pharm Biotechnol. 2004; 5:529–537. [PubMed: 15579042]
49. Silva AC, Bock NA. Manganese-enhanced MRI: an exceptional tool in translational neuroimaging. Schizophr Bull. 2008; 34:595–604. [PubMed: 18550591]
50. Strijkers GJ, Mulder WJ, van Tilborg GA, Nicolay K. MRI contrast agents: current status and future perspectives. Anticancer Agents Med Chem. 2007; 7:291–305. [PubMed: 17504156]
51. Pautler RG. Biological applications of manganese-enhanced magnetic resonance imaging. Methods Mol Med. 2006; 124:365–386. [PubMed: 16506430]
52. Elizondo G, Fretz CJ, Stark DD, Rocklage SM, Quay SC, Worah D, Tsang YM, Chen MC, Ferrucci JT. Preclinical evaluation of MnDPDP: new paramagnetic hepatobiliary contrast agent for MR imaging. Radiology. 1991; 178(1):73–78. [PubMed: 1898538]
53. Rocklage SM, Cacheris WP, Quay SC, Hahn FE, Raymond KN. Manganese(II) N,N′-Dipyridoxylethylenediamine-N,N′-diacetate 5,5′-Bis(phosphate). Synthesis and Characterization of a Paramagnetic Chelate for Magnetic Resonance Imaging Enhancement. Inorg Chem. 1989; 28:477–485.
54. Takehara Y, Sakahara H, Masunaga H, Isogai S, Kodaira N, Takeda H, Saga T, Nakajima S, Sakata I. Tumour enhancement with newly developed Mn-metalloporphyrin (HOP-9P) in magnetic resonance imaging of mice. Br J Cancer. 2001; 84:1681–1685. [PubMed: 11401324]
55. Atanasijevic T, Zhang X, Lippard SJ, Jasanoff A. MRI sensing based on the displacement of paramagnetic ions from chelated complexes. Inorg Chem. 2010; 49:2589–2591. [PubMed: 20141114]
56. Lis T. Preparation, structure, and magnetic properties of a dodecanuclear mixed-valence manganese carboxylate. Acta Crystallogr, Sect B: Struct Crystallogr Cryst Chem. 1980; 36:2042.

57. Caneschi A, Gatteschi D, Sessoli R, Barra A-L, Brunel L-C, Guillot M. Alternating current susceptibility, high field magnetization, and millimeter band EPR evidence for a ground S = 10 state in [Mn12O12(Ch3COO)16 (H2O)4].2CH3COOH.4H2O. J Am Chem Soc. 1991; 113:5873.

58. Sessoli R, Gatteschi D, Caneschi A, Novak M. Magnetic bistability in a metal-ion cluster. Nature. 1993; 365:141.

59. Christou G, Gatteschi D, Hendrickson D, Sessoli R. Single-molecule magnets. MRS Bull. 2000:25–66.

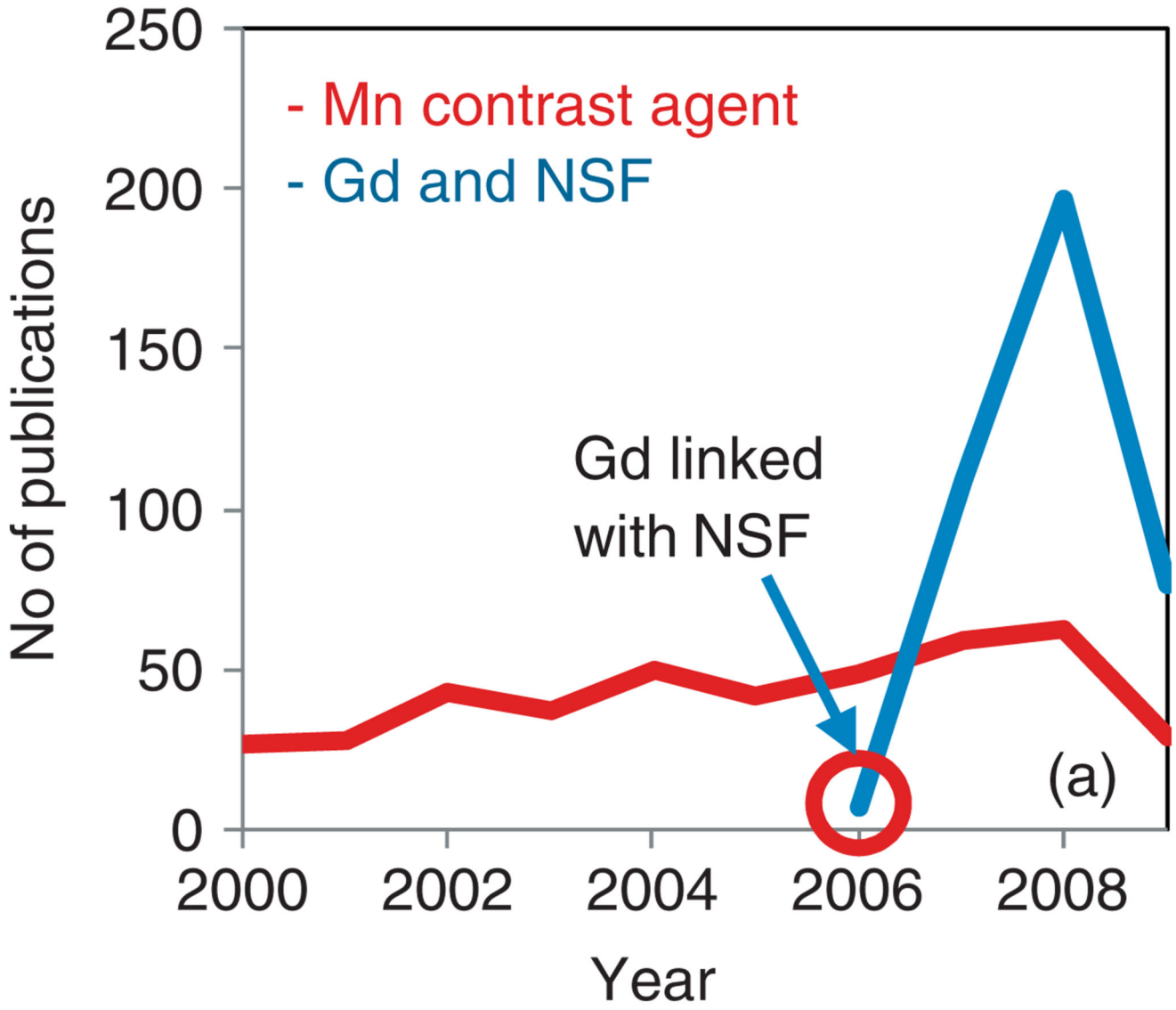

FIGURE 1.
Publication trend from Scopus: surge in publication related to Gd and NSF.

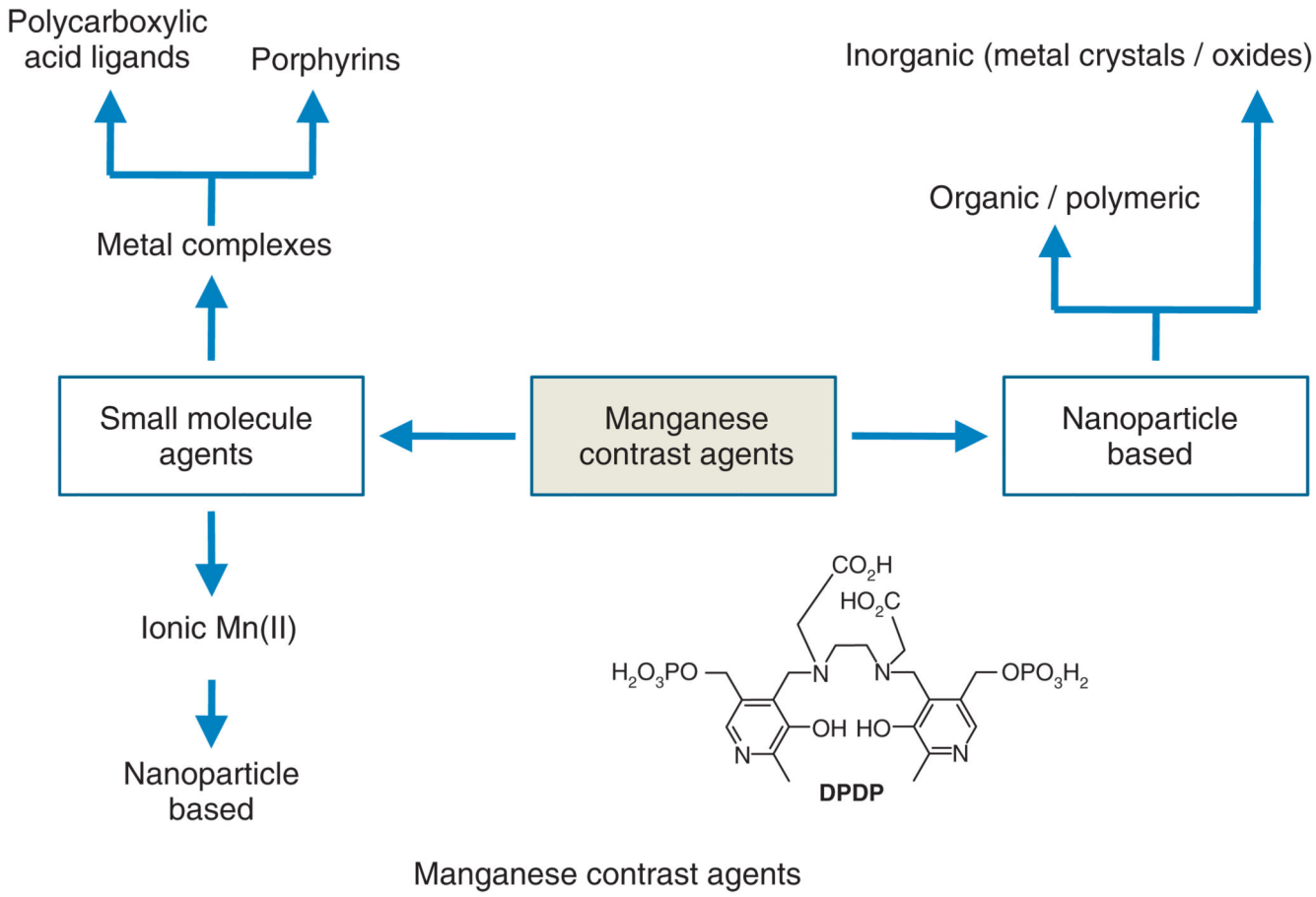

FIGURE 2.

Manganese-based contrast agent families. Inset: Structure of dipyridoxal diphosphate (DPDP), the clinically approved manganese (II) agent for hepatobiliary imaging.

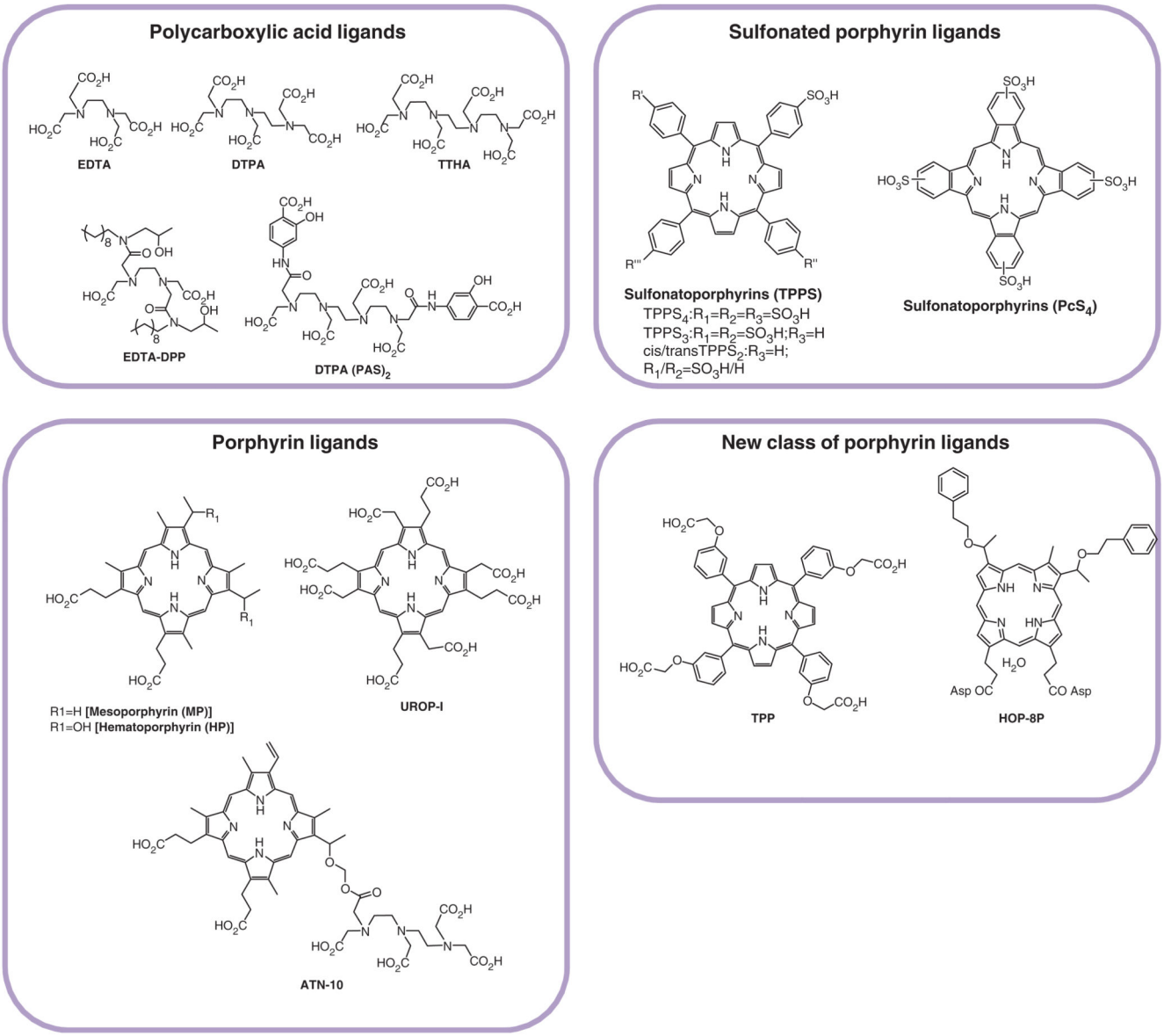

FIGURE 3.

Structures of polycarboxylates and porphyrins used as ligands for manganese.

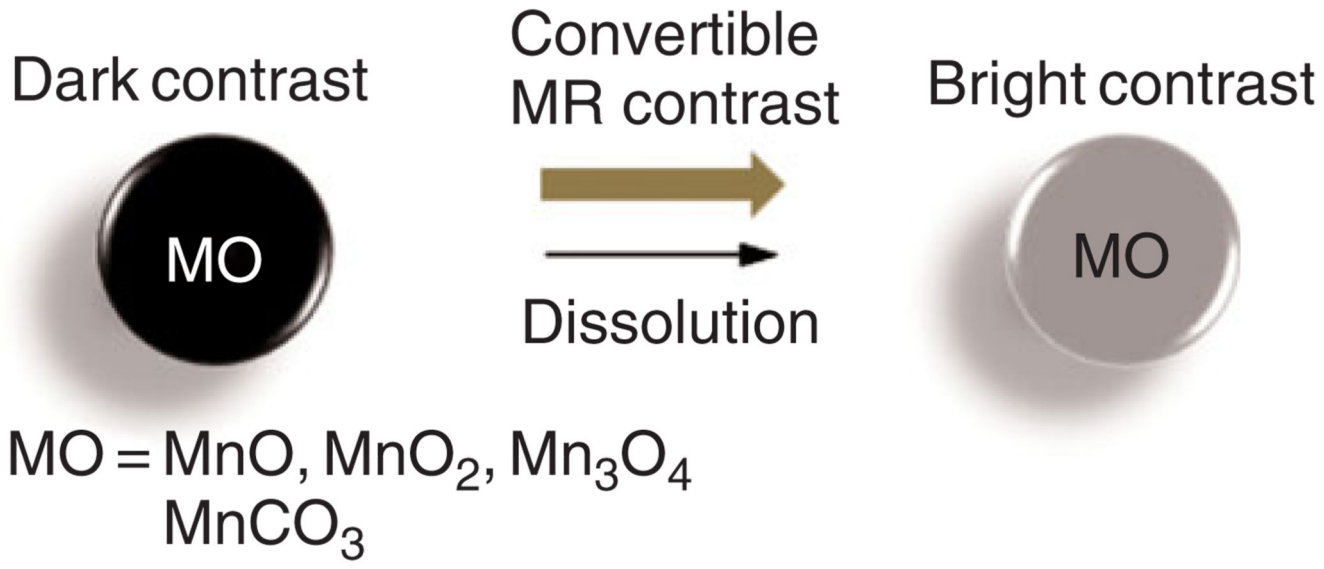

FIGURE 4.
Example of convertible inorganic contrast agents.

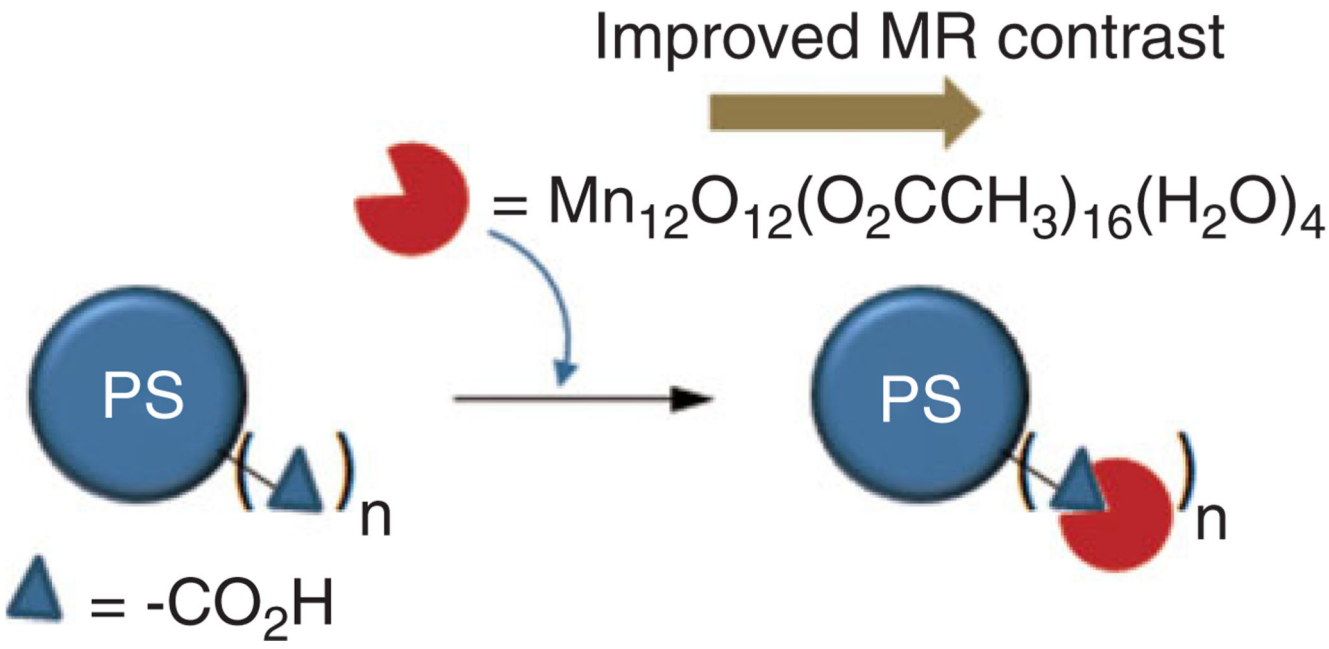

FIGURE 5.
Surface attached manganese-oxo clusters improve MR contrast (PS: polystyrene beads).

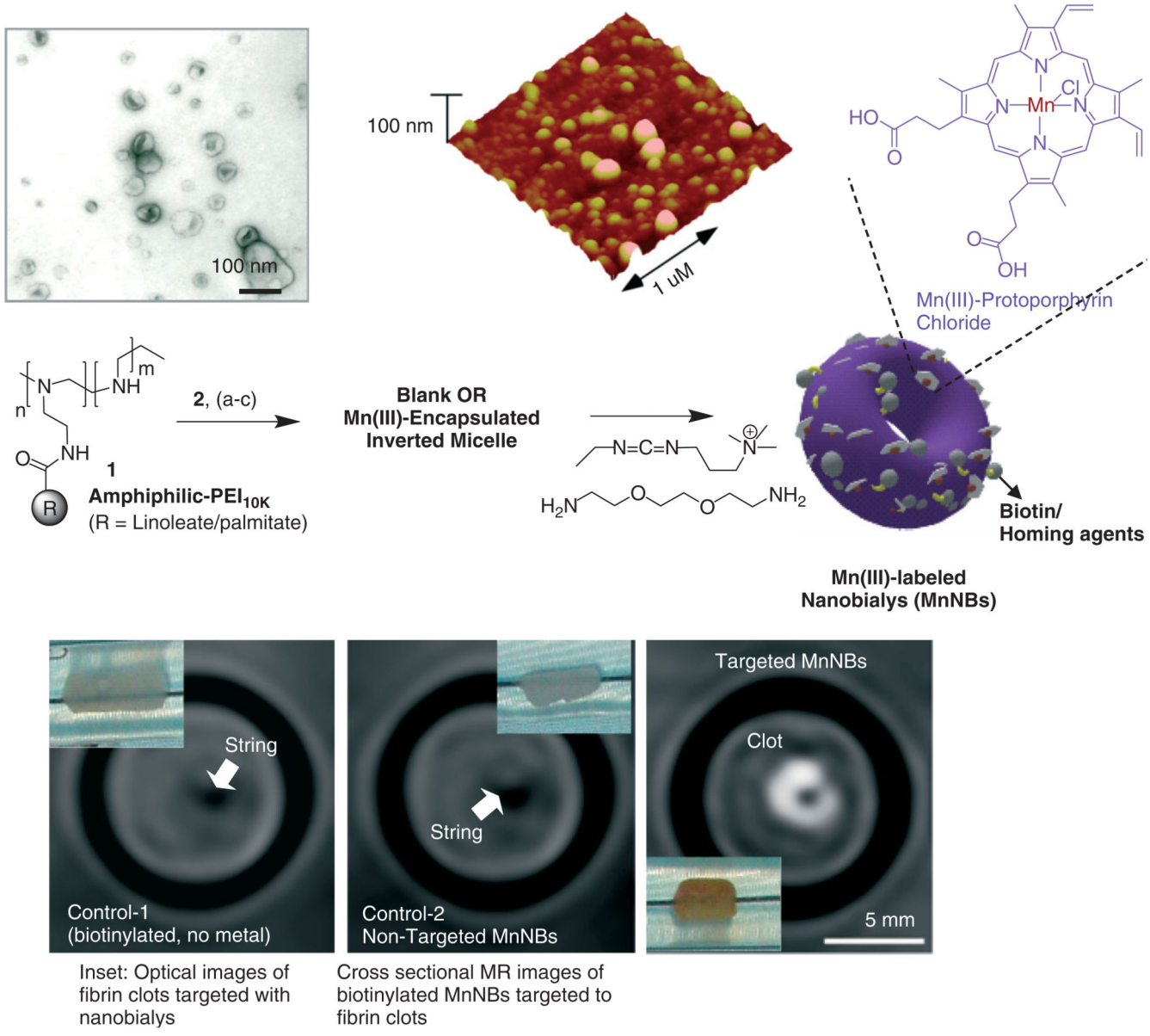

FIGURE 6.

Preparation and characterization of manganese nanobialys: (Top left) TEM (drop deposited over nickel grid, 1% uranyl acetate) and (top right) atomic force microscope (AFM) image of nanobialys (drop deposited over glass) Reaction conditions: (1) anhydrous chloroform, gentle vortexing, room temperature; (2) aqueous solution of 2 [Mn(III)-protoporphyrin], inversion, room temperature, filter using short bed of sodium sulfate and cotton; (3) Biotin-Caproyl-PE, filter mixed organic solution using cotton bed, 0.2 μM water, vortex, gently evaporation of chloroform at 45°C, 420 mbar, 0.2 μM water, sonic bath, 50°C, 1/2 h, dialysis (2 kDa MWCO cellulose membrane) against water. (Bottom) MRI images of fibrin-targeted nanobialys (right) or control nanoparticles (bottom left) and (bottom middle) bound to cylindrical plasma clots measured at 3 T.

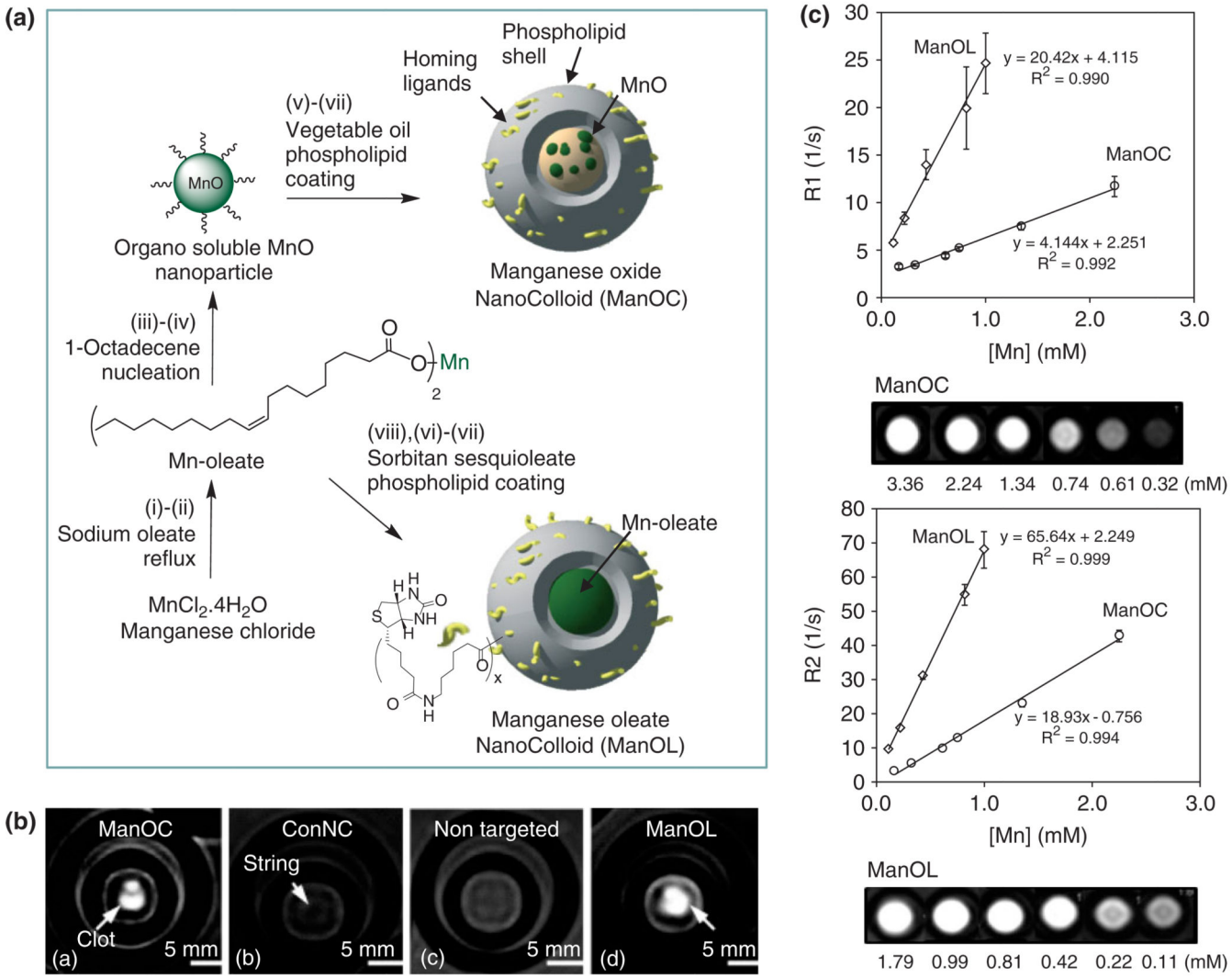

FIGURE 7.

Preparation and characterization of manganese nanocolloids: Reaction conditions: (A) Preparation of ManOC and ManOL. (i)–(ii) sodium oleate, reflux, stirring; (iii)–(iv) 1-octadecene, 325°C/70 min, stirring; (v) suspended with vegetable oil (2 w/v%), vortex, mixing; evaporation of chloroform under reduced pressure, 45°C; (vi) thin film formation from phospholipids mixture; (vii) homogenization, 20,000 psi, 4 min, 0°C; (viii) Mn-oleate, suspended with sorbitan sesquioleate (>2 w/v%), vortex, mixing, evaporation of chloroform under reduced pressure, 45°C; then steps (vi), followed by (vii). (B) MRI images of fibrin-targeted nanocolloids: (a) ManOC; (b) ConNC; (c) nontargeted-ManOL and (d) ManOL, bound to cylindrical plasma clots measured at 3 T (pixel dimension: 0.73 mm × 0.73 mm × 5 mm slice thickness). (C) MR characterization of ManOC and ManOL in suspension: (top) ionic $R1$ and (bottom) $R2$ relaxivity. The measured $R1$ relaxation rate at 3 T for ManOC (circles) and ManOL (diamonds) as a function of manganese concentration. (Reproduced with permission from Ref 38. Copyright 2009 American Chemical Society).

TABLE 1

Types of Ligands and Their Application in MR

Types of Ligands	*R*1 (MagneticField) $mM^{-1}\ s^{-1}$(MHz)	Use/Animal Model	References
Polycarboxylic acid ligands			
EDTA/EDTA-DPP	37.4 (20 MHz) (in liposomes)	Rat carcinoma	16
EDTA-BOM	55 (20 MHz)	In suspension/*in vitro*	17
EDTA-diphenylcyclohexyl	Buffer: 5.8 (20 MHz)	*In vivo* (rabbit carotid artery injury)	18
	Rabbit plasma: 51		
	Human plasma: 46		
DTPA-SA	Higher relaxivity that Gd vesicles due to the slow release of Mn(II)	Dog liver	19
TTHA	5.5 $mM^{-1}s^{-1}$ (10 MHz)	*In vitro*	20
Porphyrins (sulfonatoporphyrins)			21
PcS_4	10.10 (10.7 MHz)	Mice (human breast carcinoma)	22,23
$TPPS_4$	10.36 (20 MHz)	Rat brain gliomas and other models	22,23
$TPPS_3$	Mn-$TPPS_3$ demonstrates the greatest relaxivity among other sulfonated porphyrins	Subcut. mammary carcinoma (SMT-F) and MCF-7 human breast carcinoma	22,23
$TPPS_2$			22,23
Mesoporphyrin	1.9 (20 MHz)	Hepatobiliary contrast agent	24
Hematoporphyrin		Rat liver	25,26
UROP-1	4.75 (10 MHz)	Rat cerebral gliomas	24
ATN-10		Brain tumor, cold injury model and cytotoxic brain edema	27
TPP	13.0 (20 MHz)	Hepatocellular carcinomas	
HOP-8P		Tumor-bearing (SCC-VII) mice	27,28

EDTA, ethylenediaminetetraacetic acid; DPP, dipeptidyl peptidases; BOM, benzyloxymethyl; DTPA, diethylenetriaminepentaacetic acid; TPPS, tetraphenylporphine sulfonate, UROP-1, URO porphyrin-1, TPP, tetraphenyl porphyrin.

TABLE 2

Types of Manganese Nanoparticles/Macromolecules and Their Application in MR

Types of Nanoparticles	Magnetic Field (*R*1) T/MHz (mM^{-1} s^{-1})	Use/Animal Model	References
Inorganic particle/bulk materials			
MnO, MnO_2, Mn_3O_4, $MnCO_3$	4.0 T (in suspension) and 11.7 T (*in vitro*)	*In vitro* (mouse embryonic fibroblasts) and *In vivo* (rats)	29
Mn-doped iron oxide nanoparticle			
Mn-Fe oxide composite of rod, wire and needle shape (400–1000 nm)	1.5 T (*in vitro*) Nanoneedles: 20.81 ± 0.58; nanorods: 8.10 ± 0.31; nanowires: 6.62 ± 0.42	*In vitro* [monocyte/macrophage cell line (RAW264.7)]	30
Mn-doped SPIO coated with mPEG-*b*-PCL	1.5 T (T2 relaxivity): 270 (Mn + Fe)	*In vivo* (liver imaging mice)	31
Multifunctional magneto-polymeric nanohybrids (MMPNs)	1.5 T (T2 relaxivity): 567 (Mn + Fe)	In vitro (NIH3T 6.7 cells) and *in vivo* (mice implanted with NIH3T 6.7 cells)	32
Manganese clusters			
'Single molecule magnet' $[Mn_{12}O_{12}(O_2CCH_3)_{16}(H_2O)_4]$	47 nm: 22.0 ± 2.5 120 nm: 28.3 ± 2.0 209 nm: 37.5 ± 4.5	In suspension	33
MnPOMs: $MnSiW_{11}$ and MnP_2W_{17}	400 MHz ($MnSiW_{11}$ 12.1 and MnP_2W_{17} 4.7)	*In vivo* (healthy Wistar rats)	34
Manganese organic frames			
Mn-NMOFs	9.4 T (*r*1: 4.0 and *r*2: 112.8)	*In vitro* [human colon cancer (HT-29)]	35
MnO-based nanoparticle approach			
PEG-coated MnO	For a 15 nm particle (*r*1: 0.18; *r*2: 0.57)	*In vivo* (mice bearing the breast cancer brain metastatic tumor)	36
HMONs and WMONs	WMON: *r*1 = 0.21, *r*2 = 1.49; HMON: *r*1 = 1.42, *r*2 = 7.74	*In vivo* (mouse brain imaging)	37
Phospholipid-coated MnO	3.0 T (*r*1: 4.1; *r*2: 18.9)	*In vitro* (fibrin plasma clot)	38
Polymeric and 'Soft' particle approach			
Manganese oleate nanocolloids	3.0 T (*r*1:14.6; *r*2:70.7)	*In vitro* (fibrin plasma clot)	38
'NanoBialys' [Mn(III)-loaded polymeric agent]	1.5 T (*r*1: 3.7; *r*2: 5.2)	*In vitro* (fibrin plasma clot)	39
Dendritic manganese DTPA	4.7 T (*T*1: 4.2)	*In vitro, in vivo* (rat brain)	40

SPIO, superparamagnetic iron oxide; Mn-NMOFs, manganese-based nanoscale metal-organic frameworks; mPEG-*b*-PCL, mPolyethylenglycol-b-polycaprolactone; HMONs, hollow manganese oxide nanoparticles; PEG, polyethyleneglycol; WMONs, water-dispersible manganese oxide nanoparticles.